

# A comparison of schemes for the numerical approximation of the gyroaveraging operator

by

Oren Bassik

A dissertation submitted in partial fulfillment

of the requirements for the degree of

Master of Science

Department of Mathematics

New York University

May 2021

---

Professor Antoine Cerfon



# Abstract

The gyroaverage operator, or 2d spherical mean transform, transforms a bivariate function by averaging values over circles of (potentially large) radius. This operator has applications in plasma simulation as well as medical imaging, and its naive calculation for large radii is not well-tuned for modern, cache-sensitive processors. We implement and benchmark a variety of schemes for calculating gyroaverages in the 2D, compactly supported non-periodic setting. Schemes implemented include bilinear spline collocation, bicubic spline collocation, padded (bivariate) FFT interpolation, and bivariate tensor Chebyshev interpolation. In particular we quantify the impact of shared-memory parallelism and the use of GPU accelerators to speed up calculations, as well as the trade-off of accuracy vs computational cost, for both smooth functions and those with singularities.

# Contents

Abstract . . . . .	iii
List of Figures . . . . .	v
List of Tables . . . . .	vi
<b>1 Introduction</b>	<b>1</b>
1.1 Background . . . . .	1
1.2 Outline . . . . .	2
<b>2 Background</b>	<b>3</b>
2.1 Harmonic Analysis . . . . .	3
2.2 Harmonic Analysis of the Spherical Mean . . . . .	4
2.3 Chebyshev Approximation . . . . .	5
<b>3 Four discretizations</b>	<b>7</b>
3.1 Defining the problem . . . . .	7
3.2 Bilinear interpolation . . . . .	8
3.3 Bicubic Interpolation . . . . .	10
3.4 Fourier transform based gyroaveraging . . . . .	11
3.5 Chebyshev Spectral gyroaveraging . . . . .	12
<b>4 Design Considerations</b>	<b>17</b>
4.1 Objectives . . . . .	17
4.2 Design decisions . . . . .	17
<b>5 Numerical Results</b>	<b>22</b>
5.1 Gallery of test functions . . . . .	22
5.2 Testing environment and setup . . . . .	23
5.3 Performance and Convergence Plots . . . . .	24
5.4 Discussion of numerical results . . . . .	24
<b>6 Conclusion</b>	<b>30</b>
6.1 Proof of concept . . . . .	30
6.2 Further development . . . . .	30

# List of Figures

5.1	Gallery of test functions . . . . .	23
5.2	Gyroaveraging speed vs grid size . . . . .	25
5.3	Gyroaveraging error vs grid size . . . . .	26
5.4	The trade-off between accuracy and execution speed. . . . .	27
5.5	The benefit from GPU acceleration . . . . .	28

# List of Tables

# Chapter 1

## Introduction

### 1.1 Background

Given a function  $f$  taking real or complex values on some domain in  $\mathbb{R}^2$ , and an additional parameter specifying a radius  $\rho$ , define the gyroaveraging operator as

$$\mathcal{G}(f)(x, y; \rho) = \frac{1}{2\pi} \int_0^{2\pi} f(x + \rho \sin(\gamma), y + \rho \cos(\gamma)) \, d\gamma$$

This operator is a special case of what is called in various texts a spherical mean operator, peripheral mean operator, or spherical Radon transform. The spherical mean transform is defined for any dimension  $n \geq 1$  as

$$\mathcal{J}(f)(\mathbf{x}; \rho) = \frac{1}{\omega_n} \int_{|\mathbf{y}|=1} f(x + \rho \mathbf{y}) \, dS(\mathbf{y}) = \oint_{\partial B(\mathbf{x}, \rho)} f(\mathbf{y}) \, dS(\mathbf{y})$$

This operator is introduced in many PDE textbooks (see, for instance, [4, p. 67]), among other applications, to solve the wave equation in  $n$  dimensions. Our interest in the numerical calculation of the 2D case, as well as the name “gyroaverage”, comes from an application in plasma physics: solving the “Vlasov-Poisson” equations to simulate a beam of charged particles in a cyclotron. While a detailed derivation is out of the scope of this thesis, and is described in detail in [6], a very brief description of the scheme is given (in [6]) as:

Briefly, our method of solution of the VPE consists of the following steps: (1) calculate  $\mathcal{G}f$  via various numerical algorithms, (2) compute  $\chi$  with a free-boundary Poisson solver, and (3) time-advance  $f$  in the Vlasov equation.

The Poisson solver and time-stepping parts of the solver are well-studied and have many well-known schemes (as well as many freely available implementa-

tions); meanwhile the gyroaveraging operator is being applied inside the time-stepping loop and suffers from (as is apparent from the definition) “everywhere-to-everywhere” dependence. Thus it is reasonable to expect gains from speeding up the gyroaveraging as the lowest hanging fruit in improving this particular solver.

Another application (described in [5] and [3]) is in the field of thermoacoustic tomography. Very briefly, an electromagnetic radiation source is applied to a body of biologic tissue, which generates heat pulses in the tissue; this in turn causes small, temporary expansions. These expansions radiate outwards as sound waves, and are detected at the boundary of the tissue by an array of transducers. The reconstruction of an image from the transducer signals is, mathematically, a problem of inverting the spherical mean transform. One angle of attack for the inverse problem is via iterative methods, which rely on applying the forward transform to repeatedly refine potential inverses; for these methods efficient and scalable algorithms for the forward transform translate into gains for the inverse.

## 1.2 Outline

In the remainder of this paper, we will focus on the forward gyroaveraging operator alone, in a 2D setting. We assume that we are in the context of a numerical solver, and that we have access to function values alone (and not an analytic representation), and that our domain of interest is bounded (i.e. we are gyroaveraging functions of compact support.)

Chapter 2 will recall some basic facts needed for the rest of the paper, including: Fourier analysis, Chebyshev approximation theory and spline approximation, as well as basic properties of the spherical mean transform.

Chapter 3 will describe the four different discretizations which we implemented, and the mathematical operation of applying the gyroaverage operator onto each. In the case of smooth functions, we present some error estimates.

Chapter 4 adds implementation details, and addresses design considerations from the computer science perspective. Included is a very brief overview of the API implemented.

Chapter 5 presents numerical results; we start by defining four functions with different salient features and in each case analyze converge and calculation speed, for each implemented algorithm.

Chapter 6 summarizes the numerical results and outlines areas for further improvement and investigation.



# Chapter 2

## Background

We use this chapter to record some basic facts we will use later. Mainly we will be quoting from references.

### 2.1 Harmonic Analysis

The below follows the notation and presentation from the expanded edition of [10], which includes the appendix “ATAP for Periodic Functions.” Let  $f$  be a Lipschitz continuous periodic function defined on  $[0, 2\pi]$ . Then  $f$  is associated to a Fourier series

$$f(t) = \sum_{k=-\infty}^{k=\infty} c_k e^{ikt}$$

where the coefficients are given by the formula

$$c_k = \frac{1}{2\pi} \int_0^{2\pi} f(t) e^{-ikt} dt.$$

We can truncate this expansion:

$$f_n(t) = \sum_{k=-n}^n c_k e^{ikt}$$

which is an approximation to  $f$ , the “degree  $n$  trigonometric projection” of  $n$ . In practice, we may not have access to the exact coefficients  $c_k$ , but must rely only on values of  $f$  sampled at  $N$  points, generally equispaced in  $[0, 2\pi]$ . Let  $f_j = f\left(\frac{2\pi j}{N}\right)$ . Then we can use the formula

$$\tilde{c}_k = \frac{1}{N} \sum_{j=0}^{N-1} f_j e^{-ikt}$$

which gives, via the same truncated expansion as above, the “trigonometric interpolant”  $p_n$  to  $f$ .

Now, if  $f$  satisfies some smoothness condition, a standard argument involving repeated integration by parts yields the below error bounds. This is Theorem B.2 in [10, Appendix B].

**Theorem B.2.** *If  $f$  is  $\nu \geq 1$  times differentiable and  $f^{(\nu)}$  is of bounded variation  $V$  on  $[0, 2\pi]$ , then its degree  $n$  trigonometric projection and interpolant satisfy*

$$\|f - f_n\|_\infty \leq \frac{V}{\pi\nu n^\nu}, \quad \|f - p_n\|_\infty \leq \frac{2V}{\pi\nu n^\nu}$$

*If  $f$  is analytic with  $|f(t)| \leq M$  in the open strip of half-width  $\alpha$  around the real axis in the complex  $t$ -plane, they satisfy*

$$\|f - f_n\|_\infty \leq \frac{2Me^{-\alpha n}}{e^\alpha - 1}, \quad \|f - p_n\|_\infty \leq \frac{4Me^{-\alpha n}}{e^\alpha - 1}$$

## 2.2 Harmonic Analysis of the Spherical Mean

Our interest in Fourier analysis is justified by the following calculation, which shows how the gyroaverage is greatly simplified in frequency space. We focus on the bivariate case. Suppose we have a Lipschitz continuous function  $f$  on  $\Omega = [0, 2\pi]^2$ , which is continuous and doubly periodic. We have the Fourier series

$$f(x, y) = \sum_{k=-\infty}^{\infty} \sum_{\ell=-\infty}^{\infty} c_{k,\ell} e^{2\pi i(kx + \ell y)}$$

where

$$c_{k,\ell} = \int_0^{2\pi} \int_0^{2\pi} f(t_1, t_2) e^{-2\pi i(kt_1 + \ell t_2)} dt_1 dt_2$$

If we recall the definition of the gyroaverage

$$\mathcal{G}(f)(x, y; \rho) = \frac{1}{2\pi} \int_0^{2\pi} f(x + \rho \sin(\gamma), y + \rho \cos(\gamma)) d\gamma$$

We can ask what happens to a Fourier basis function under this operator. Let

$$f_{k,\ell}(x, y) = e^{2\pi i(kx + \ell y)}$$

Then

$$\mathcal{G}(f_{k,\ell}) = \frac{1}{2\pi} \int_0^{2\pi} f_{k,\ell}(x + \rho \sin(\gamma), y + \rho \cos(\gamma)) d\gamma =$$

$$\frac{1}{2\pi} \int_0^{2\pi} e^{2\pi i(k(x+\rho \sin \gamma) + \ell(y+\rho \cos \gamma))} d\gamma = \frac{e^{2\pi i(kx+\ell y)}}{2\pi} \int_0^{2\pi} e^{2\pi i\rho(k \sin \gamma + \ell \cos \gamma)} d\gamma =$$

$$f_{k,\ell} \frac{1}{2\pi} \int_0^{2\pi} e^{2\pi i\rho(k \sin \gamma + \ell \cos \gamma)} d\gamma$$

Next we use the identity  $k \sin \gamma + \ell \cos \gamma = C \cos(\gamma + \phi)$ , where  $C = \sqrt{k^2 + \ell^2}$  and  $\phi = \tan^{-1}(-\frac{k}{\ell})$ . The above is then

$$\mathcal{G}(f_{k,\ell}) = f_{k,\ell} \frac{1}{2\pi} \int_0^{2\pi} e^{2\pi i\rho C \cos(\gamma+\phi)} = f_{k,\ell} \cdot J_0(2\pi\rho\sqrt{k^2 + \ell^2})$$

Where  $J_0(\cdot)$  is a Bessel function of the first kind, and the above is one form of the “integral representation” found, e.g. in [1] or [2, Eq 10.9.17]. Applied to the Fourier series expansion of an arbitrary function  $f$ , we see that

$$\mathcal{G}(f)(x, y; \rho) = \sum_{k=-\infty}^{\infty} \sum_{\ell=-\infty}^{\infty} J_0(2\pi\rho\sqrt{k^2 + \ell^2}) c_{k,\ell} e^{2\pi i(kx+\ell y)}$$

This is expected, as the gyroaverage is a form of convolution; in Fourier space the operator is computed simply by a multiplier that depends only on  $(\rho, k, \ell)$ . This fact is true, with similar derivation and slightly different Bessel functions, for all dimensions and for continuous Fourier transforms as well.

## 2.3 Chebyshev Approximation

A full review of Chebyshev polynomials and their use in approximation theory is beyond the scope of this paper, and the primary subject of [10]. For one who is comfortable with Fourier analysis, the easiest point of view is that to approximate a function  $f$  on  $[-1, 1]$ , wrap it around the unit circle by the transform

$$\theta = \cos^{-1} x$$

Then  $f(\cos(\theta))$  is a periodic, even function of  $\theta$  which is then subject to decomposition and approximation by (cosine) Fourier methods. We quote 3 theorems, all from [10] which are analogous to the results for Fourier series above.

Define the Chebyshev polynomials as

$$T_k(x) = \cos(k \cos^{-1}(x))$$

Then any Lipschitz continuous function on  $[-1, 1]$  has a representation

$$f(x) = \sum_{k=0}^{\infty} a_k T_k(x)$$

with

$$a_k = \frac{2}{\pi} \int_{-1}^1 \frac{f(x)T_k(x)}{\sqrt{1-x^2}} dx$$

except that  $\frac{2}{\pi}$  becomes  $\frac{1}{\pi}$  for  $k = 0$ . We can truncate this series and obtain

$$f_n(x) = \sum_{k=0}^n a_k T_k(x)$$

or, in analogy to the Fourier case, we can admit that in practice we may not have access to the integrals defining  $a_k$ . Then we sample at Chebyshev nodes,  $x_j = \cos\left(\frac{j\pi}{n}\right)$  and interpolate to find coefficients  $c_k$ , such that

$$p_n(x) = \sum_{k=0}^n c_k T_k(x)$$

satisfies  $p_n(x_j) = f(x_j)$ . (This interpolation is a discrete cosine transform, and is handled efficiently by FFT-based algorithms.) Then we have the following theorems bounding the error of the above, quoted from [10]. We will not pause to define every term, and indeed Bernstein ellipses are somewhat technical. The moral is that smoother functions will have faster convergence from interpolants than less smooth functions.

**Theorem 7.2 Convergence for differentiable functions.** *For any integer  $\nu \geq 0$ , let  $f$  and its derivatives through  $f^{\nu-1}$  be absolutely continuous on  $[-1, 1]$  and suppose the  $\nu$ th derivative is of bounded variation  $V$ , then for any  $n > \nu$ , the Chebyshev projections satisfy*

$$\|f - f_n\| \leq \frac{2V}{\pi\nu(n-\nu)^\nu}$$

and its Chebyshev interpolants satisfy

$$\|f - p_n\| \leq \frac{4V}{\pi\nu(n-\nu)^\nu}$$

**Theorem 8.2 Convergence for analytic functions.** *Let a function  $f$  analytic in  $[-1, 1]$  be analytically continuable to the open Bernstein ellipse  $E_\rho$ , where it satisfies  $|f(x)| \leq M$  for some  $M$ . Then for each  $n \geq 0$  its Chebyshev projections satisfy*

$$\|f - f_n\| \leq \frac{2M\rho^{-n}}{\rho - 1}$$

and its Chebyshev interpolants satisfy

$$\|f - p_n\| \leq \frac{4M\rho^{-n}}{\rho - 1}$$

# Chapter 3

## Four discretizations

### 3.1 Defining the problem

We proceed by defining precisely the problem we are solving, and the four discretizations we have implemented.

The input data are

1. A function  $f(x, y, \rho) : [-1, 1]^2 \times [0, 2] \rightarrow \mathbb{R}$
2. A set of  $\rho_k \in [0, \infty)$  which represent gyroradii;
3. We choose a set of  $N^2$  nodes  $(x_i, y_j)$  with  $x_i, y_j \in [-1, 1], 1 \leq i, j \leq N$ .
4. We are then given the values of  $f$  at each of the nodes  $x_i, y_j, \rho_k$ .

We assume the function is identically 0 outside of the box  $[-1, 1]$  but that it may have nonzero derivatives on the boundary. The two choices of input nodes  $x_i$  and  $y_i$  we investigate are

1. equispaced nodes
2. Chebyshev nodes

We then want to populate, for each  $\rho_k$ , a matrix  $\mathcal{G}(f)$  with approximations to

$$(\mathcal{G}f)_{\rho_k}(x'_i, y'_j) = \frac{1}{2\pi} \int_0^{2\pi} f(x'_i + \rho_k \sin(\gamma), y'_j + \rho_k \cos(\gamma)) d\gamma.$$

Where the primed  $x'_i, y'_j$  are equispaced nodes in every case (even when we sample at Chebyshev nodes to begin with.) The choice of identical output space allows for uniform comparison of convergence between schemes, and it turns out it does not

penalize the Chebyshev scheme. For the remainder of this chapter we will suppress the variable  $\rho_k$  and treat  $f$  as a bivariate function.

It will be critical for convergence analysis to point out a potentially “aphysical” feature of how we have defined the problem. Implicit in the above is a hard boundary around the unit square, and we assume a discontinuous drop to 0 for  $f$  outside the unit square in the definition of our average. Indeed we could have made this explicit with an indicator function inside the integral.

Given that the problem is basically a quadrature problem, we proceed as many quadrature schemes do: we interpolate between the given samples and try to integrate the interpolant exactly. We have implemented four different interpolation schemes, which we detail one by one below.

## 3.2 Bilinear interpolation

Our simplest interpolation is bilinear. Given equispaced nodes, on each rectangle  $[x_i, x_{i+1}] \times [y_j, y_{j+1}]$   $f$  is represented by the unique polynomial of the form  $A + Bx + Cy + Dxy$  which matches the sampled value at each corner. This is a continuous but not necessarily differentiable approximation of  $f$ . One can express the map from sampled values to parameters  $(A, B, C, D)$  as a matrix, or compute interpolating values (for points between samples) on the fly.

Given bilinear interpolation, we have two algorithms which produce (roughly) the same mathematical quadrature but differ greatly in speed. The first algorithm is to set up the bilinearly interpolated values of  $f$  as a function  $\tilde{f}$  and feed this function into a black-box adaptive integration algorithm (we use an adaptive Gauss-Kronrod quadrature from the C++ Boost library; further details in chapter 4).

The second algorithm is one of the main innovations of this paper (and was suggested, more or less in full, by Prof. Cerfon.) It has a modestly expensive precomputation step after which the gyroaveraging itself is represented by a sparse matrix which can be applied directly to the sample values matrix. We describe first the precomputation with reference to figure TODO:

1. Fix a particular  $x_c, y_c$  and  $\rho$  of interest. We want to approximate

$$\mathcal{G}f(x_c, y_c) = \frac{1}{2\pi} \int_0^{2\pi} f(x_c + \rho \sin(\gamma), y_c + \rho \cos(\gamma)) d\gamma$$

2. Enumerate the points of intersection between the circle  $(x_c + \rho \sin \gamma, y_c -$

$\rho \cos \gamma$ ) and the grid lines  $x = x_i$  and  $y = y_j$ . This will produce a vector of angles  $(\gamma_0 = 0, \gamma_1, \dots, \gamma_p = 2\pi)$  such that

- (a) Each arc corresponding to  $[\gamma_i, \gamma_{i+1})$  lies entirely between grid lines, and so is represented by a single bilinear polynomial in that region
- (b) The disjoint union of the arcs is the entire circle

Thus

$$\begin{aligned} \mathcal{G}f(x_c, y_c) &= \frac{1}{2\pi} \sum_p \int_{\gamma_p}^{\gamma_{p+1}} f(x_c + \rho \sin(\gamma), y_c + \rho \cos(\gamma)) d\gamma \approx \\ &\sum_p \int_{\gamma_p}^{\gamma_{p+1}} \tilde{f}_p(x_c + \rho \sin(\gamma), y_c + \rho \cos(\gamma)) d\gamma \end{aligned}$$

where

$$\tilde{f}_p(x, y) = A_p + B_p x + C_p y + D_p xy$$

We can analytically integrate, indeed

$$\begin{aligned} &\int \tilde{f}_p(x_c + \rho \sin(\gamma), y_c + \rho \cos(\gamma)) d\gamma = \\ &A_p \gamma + B_p(\gamma x_c - \rho \cos \gamma) + C_p(\gamma y_c - \rho \sin \gamma) + \frac{D_p}{2}(\rho^2 \cos^2 \gamma + 2x_c y_c \gamma - 2\rho y_c \cos \gamma - 2\rho x_c \sin \gamma) \end{aligned}$$

Thus the contribution of each arc to the total gyroaverage is seen to be linear in the coefficients  $A_p, B_p, C_p, D_p$ .

3. These coefficients are themselves a linear combination of the sample values at the corners of the grid rectangle containing each arc. For each arc, compose two matrices to find the contribution of that arc to  $\mathcal{G}f(x_c, y_c)$  as a linear function of sample values.
4. Form a sparse  $N^2 \times N^2$  matrix which operates on sample values and outputs the matrix  $\mathcal{G}f(x_c, y_c)$  flattened as a vector. More precisely, each row represents one gyroaverage circle, and there will be 4 nonzero entries representing each arc in each row.

The number of nonzero entries in the resulting sparse matrix is  $O(N^3)$ : we have  $N^2$  circles, and the number of arcs per circle is bounded by  $4N$ .

This sparse matrix can be initialized and cached, and depends only on the domain and  $\rho$ . After precomputation the actual gyroaveraging algorithm is simple: we multiply the sample value matrix by the precomputed sparse matrix. This has runtime complexity of  $O(N^3)$  and we expect it to scale very well, and to benefit from extensive prior work on sparse linear algebra. We also expect to be constrained by the accuracy of a bilinear interpolation.

### 3.3 Bicubic Interpolation

Here, using equispaced nodes, we approximate  $f$  by the form

$$\tilde{f}(x, y) = \sum_{i,j=0}^3 a_{ij} x^i y^j$$

We need choose 16 coefficients for each grid space  $[x_i, x_{i+1}] \times [y_j, y_{j+1}]$ . The most natural choice is to match values and first derivatives at each corner, as well the mixed derivative  $f_{xy}$ .

We don't have analytic derivatives available, so our code uses 4th order finite difference approximations (a 5-point stencil for  $f_x$  and  $f_y$ , and 16-point stencil for  $f_{xy}$ .) To reduce memory usage, we represent the stencil in code rather than represent the finite difference operator as a sparse matrix. After calculating finite difference approximations, we use the below formula for bicubic interpolation. There are a few standard ways to do this; the below was slightly faster than a 16x16 sparse matrix multiplication on one test machine (but this is almost certainly machine/language/compiler dependent.)

#### 3.3.1 Interpolation formula

Suppose we are interpolating on the square between  $(x_0, y_0)$  and  $(x_1, y_1)$ . Let superscripts  $f^{00}, f^{10}, f^{01}, f^{11}$  denote the sampled values of  $f$  at  $(x_0, y_0), (x_1, y_0), (x_0, y_1), (x_1, y_1)$  respectively. Similarly let  $f_x, f_y$ , and  $f_{xy}$  denote the finite difference approximations. Then if define the matrix  $\{a_{ij}\}$  as

$$\begin{pmatrix} a_{00} & a_{01} & a_{02} & a_{03} \\ a_{10} & a_{11} & a_{12} & a_{13} \\ a_{20} & a_{21} & a_{22} & a_{23} \\ a_{30} & a_{31} & a_{32} & a_{33} \end{pmatrix} = \begin{pmatrix} 1 & x_0 & x_0^2 & x_0^3 \\ 1 & x_1 & x_1^2 & x_1^3 \\ 0 & 1 & 2x_0 & 3x_0^2 \\ 0 & 1 & 2x_1 & 3x_1^2 \end{pmatrix}^{-1} \begin{pmatrix} f^{00} & f^{01} & f_y^{00} & f_y^{01} \\ f^{10} & f^{11} & f_y^{10} & f_y^{11} \\ f_x^{00} & f_x^{01} & f_{xy}^{00} & f_{xy}^{01} \\ f_x^{10} & f_x^{11} & f_{xy}^{10} & f_{xy}^{11} \end{pmatrix} \begin{pmatrix} 1 & y_0 & y_0^2 & y_0^3 \\ 1 & y_1 & y_1^2 & y_1^3 \\ 0 & 1 & 2y_0 & 3y_0^2 \\ 0 & 1 & 2y_1 & 3y_1^2 \end{pmatrix}^{-T}$$

Then the polynomial  $\sum a_{ij} x^i y^j$  matches all the appropriate values and derivatives at the corners.

#### 3.3.2 Bicubic interpolation: Precomputed matrix

For fast bicubic interpolation, we take an array with  $16N^2$  values, specifying a bicubic form for each square in the grid, and construct a sparse matrix similarly to the bilinear algorithm. For a particular  $(x_c, y_c)$  and given  $\rho$ , the gyroaverage has the same form

$$\sum_p \int_{\gamma_p}^{\gamma_{p+1}} \tilde{f}_p(x_c + \rho \sin(\gamma), y_c + \rho \cos(\gamma)) d\gamma$$



where in the bicubic case

$$\tilde{f}_p(x, y) = \sum_{i,j=0}^3 a_{ij,p} x^i y^j$$

These terms are each analytically integrable. The formulas are too large to include here. The source code that handles this integration was generated by the SAGE computer algebra system and some post-processing, about is about 100 lines of C++ code (for all 16 integrals).

In the bicubic case, we form a sparse matrix which operates on the matrix of bicubic polynomial coefficients. The breakup of circles into arcs is exactly the same as in the bilinear case. The contribution of each arc to a particular gyroaverage takes exactly four times as many parameters (and the relationship is still linear.) Thus applying this sparse matrix has the asymptotic complexity ( $O(n^3)$ ) as the previous case, and precisely four times as many nonzeros entries.

### 3.3.3 Bicubic Interpolation: Gyroaveraging

After the precomputation step, the gyroaveraging calculation has three steps:

1. Calculate finite difference approximations for  $f_x$ ,  $f_y$ , and  $f_{xy}$  (this can be represented as a stencil or a sparse matrix).
2. Solve for bicubic parameters on each grid space (this is  $16N^2$  elements)
3. Multiply bicubic parameter matrix by sparse precomputed gyroaverage operator matrix ( this is  $O(N^3)$  as discussed above)

As in the bilinear case, the precomputed sparse matrix depends only on the domain and  $\rho$ . The asymptotic complexity is the same, and the flop count almost precisely four times larger than the bilinear case. We expect similar scaling but greater accuracy from higher order interpolation.

## 3.4 Fourier transform based gyroaveraging

The next scheme is suggested by [11] and is intended for the case where  $f$  is numerically compactly supported, i.e. the function and all of its derivatives are 0 on the boundary. In this case we can view the function as periodic, in which case the conclusions of section 2.1 apply. In this case, the gyroaveraging operator is diagonal, and we we can compute a gyroaverage with the following algorithm:

1. First, pad the sample data with zeros on all sides. The size of this padding needs to be as large as the largest  $\rho$  under consideration. If we failed to pad, this algorithm would interpret  $f$  as periodic.

2. Second, transform the (padded) sample data via a 2-dimensional DCT (discrete cosine transform). If we call the padded data  $f'_{ij}$ , then we have a matrix  $a_{pq}$  and the decomposition of the sample data as

$$f'_{ij} = \sum'_{p=0}^{N-1} \sum'_{q=0}^{N-1} \hat{f}'_{pq} \cos\left(\frac{\pi p(2i+1)}{2N}\right) \cos\left(\frac{\pi q(2j+1)}{2N}\right)$$

The primed sums indicate that for  $p = 0$  or  $q = 0$  we add a  $\frac{1}{2}$  coefficient before  $\hat{f}'_{pq}$ . There are various conventions; this is the convention in the FFTW package with the parameter REDFT10.

3. Perform an entry-wise (“Hadamard”) multiplication of this matrix by the matrix  $B_{pq}$  where

$$B_{pq} = \frac{J_0\left(\left(\frac{\pi p \rho(N-1)}{Nw}\right)^2 + \left(\frac{\pi q \rho(N-1)}{Nw}\right)^2\right)}{4N^2}$$

where  $J_0$  is the Bessel function of the first kind and  $w$  is the width of the expanded domain after padding.

4. Apply the inverse discrete cosine transform (in the FFTW package, this is named “REDFT01”) to the matrix  $B_{pq} \hat{f}'_{pq}$
5. Throw out the matrix elements corresponding to the padding.

For this algorithm, we expect spectral accuracy for smooth functions where the boundary conditions are satisfied, and poor convergence (including Gibbs-style artifacts) when they are not. The algorithmic complexity is  $O(N^2 \log n)$ . The matrix of Bessel values can be precomputed and cached, and with sufficient care (and spare memory) the padding can be reused from one gyroaveraging to the next. Thus the main bottleneck in this algorithm is the extremely well optimized FFT-based DCT calculation, and scales with parallelism as the FFT does.

### 3.5 Chebyshev Spectral gyroaveraging

Our final interpolation method is bivariate Chebyshev interpolation. Here  $f$  is represented by the bivariate Chebyshev series

$$\tilde{f}(x, y) = \sum''_{p=0}^{N-1} \sum''_{q=0}^{N-1} \hat{f}_{pq} T_p(-x) T_q(-y)$$

where here the primed sums indicate the first and last coefficients are halved.

The Chebyshev series is computed stably and efficiently via a DCT, given that we have samples at the Chebyshev nodes. Indeed, let  $x_m = -\cos(\frac{m\pi}{N-1})$ ,  $y_n = -\cos(\frac{n\pi}{N-1})$ , for  $0 \leq m, n \leq N-1$ . Define the function  $D_{pq}(x, y) = a_p b_q T_p(-x) T_q(-y)$ . Here  $a_p$  and  $b_q$  are indicators which “undo” the double primed summation below;  $a_p = \frac{1}{2}$  for  $p = 0$  or  $N-1$  and  $a_p = 1$  otherwise, and the same for  $b_q$ . These are the basis functions against which we are decomposing  $f$ . We prove, below, a special case of “orthogonality relations”, i.e. that the particular DCT below, applied to one of these functions, results in a matrix with a single nonzero entry.

At any of the nodes  $(x_m, y_n)$  we have

$$D_{pq}(x_m, y_n) = a_p b_q T_p(-x_m) T_q(-y_n) = a_p b_q \cos(p \cos^{-1}(-x_m)) \cos(q \cos^{-1}(-y_n)) =$$

$$a_p b_q \cos \frac{mp\pi}{N-1} \cos \frac{nq\pi}{N-1}$$

Furthermore, define the 2D type-I DCT (named “REDFT00” in the FFTW package), given an input matrix  $f_{mn}$ , as

$$\hat{f}_{k,\ell} = \sum_{m=0}^{N-1}{}'' \sum_{n=0}^{N-1}{}'' f_{mn} \cos \frac{m\pi k}{N-1} \cos \frac{n\pi \ell}{N-1}$$

Here the double primed summation means the first and last terms are halved. Then, if we apply this transform to a basis function  $D_{pq}$  evaluated at the Chebyshev nodes, we find that

$$\hat{D}_{k,\ell} = \sum_{m=0}^{N-1}{}'' \sum_{n=0}^{N-1}{}'' D_{pq}(x_m, y_n) \cos \frac{m\pi k}{N-1} \cos \frac{n\pi \ell}{N-1} =$$

$$\sum_{m=0}^{N-1}{}'' \sum_{n=0}^{N-1}{}'' a_p b_q \cos \frac{mp\pi}{N-1} \cos \frac{nq\pi}{N-1} \cos \frac{m\pi k}{N-1} \cos \frac{n\pi \ell}{N-1} =$$

$$a_p b_q \sum_{m=0}^{N-1}{}'' \left( \cos \frac{mp\pi}{N-1} \cos \frac{m\pi k}{N-1} \left( \sum_{n=0}^{N-1}{}'' \cos \frac{nq\pi}{N-1} \cos \frac{n\pi \ell}{N-1} \right) \right) =$$

Focusing on the term inside the parenthesis, by product-to-sum for cosines, we want

$$\frac{1}{2} \sum_{n=0}^{N-1}{}'' \left( \cos \frac{n(q+\ell)\pi}{N-1} + \cos \frac{n(q-\ell)\pi}{N-1} \right)$$

Adopt the notation  $e(\theta) = e^{\frac{i\pi\theta}{N-1}}$ , let  $u = q + \ell, v = q - \ell$  then the above is

$$\frac{1}{4} \sum_{n=0}^{N-1} ((e(q + \ell))^n + (e(-q - \ell))^n + (e(q - \ell))^n + (e(-q + \ell))^n)$$

Note that for  $x \neq 1$ , we have (this is just a “primed” geometric series):

$$\sum_{n=0}^{N-1} x^n = \frac{(x + 1)(x^{N-1} - 1)}{2(x - 1)}$$

Applied here, this makes our sum

$$\begin{aligned} & \frac{1}{8} \left( \frac{(e(u) + 1)(-1^u - 1)}{e(u) - 1} + \frac{(e(-u) + 1)(-1^u - 1)}{e(-u) - 1} \right) + \\ & \frac{1}{8} \left( \frac{(e(v) + 1)(-1^v - 1)}{e(v) - 1} + \frac{(e(-v) + 1)(-1^v - 1)}{e(-v) - 1} \right) \end{aligned}$$

Since  $e(-\theta) = e(\theta)^{-1}$ , after clearing denominators the above collapses to 0. This holds whenever  $q \neq l$ . By the same argument, the summation will be 0 unless  $k = p$  as well.

The above shows that if  $f$  is given globally by

$$f(x, y) = \sum_{p=0}^{N-1} \sum_{q=0}^{N-1} a_{pq} D_{pq}(x, y)$$

Then the DCT will recover the coefficients  $a_{pq}$ . Furthermore, by decomposing  $f$  into this basis, we can compute the gyroaverage of  $f$  as the linear combination of gyroaverages of the basis functions  $D_{pq}$ . If the gyroaverages of the basis functions are known analytically, or with high precision, then error will mainly come from the Chebyshev approximation, which is spectral for smooth functions and enjoys many other extremal properties as outlined in [10], [7], and [8].

### 3.5.1 Dense Chebyshev gyroaveraging matrix: Precomputation

For this algorithm, we form as a dense matrix the operator which takes a vector (flattened 2D matrix) of Chebyshev coefficients ( $a_{pq}$  above, or  $\hat{f}_{pq}$  below) and returns a vector (also a flattened 2D matrix) of gyroaverages. This matrix is a flattened version of a 4-parameter array. The entries that need to be computed are

$$I_\rho(p, q, i, j) = (\mathcal{G}D_{pq})(x_i, y_j) = \frac{1}{2\pi} \int_0^{2\pi} T_p(x_i + \rho \sin(\gamma)) T_q(y_j + \rho \cos(\gamma)) d\gamma$$

The above needs a few points of precision however:

1. The  $x_i, y_i$  can actually be any set of points. Our code actually targets equispaced points but targeting Chebyshev nodes has the same cost.
2. The above definition is assuming that  $T_n(x)$  is defined to be identically 0 outside  $[-1, 1]$ . Alternatively we could have included an indicator function in our definition. This point is critical; we handle it in our code by specifying bounds of integration so that arcs outside the unit square are skipped.

This matrix is a dense matrix with  $N^4$  entries. It scales poorly with  $N$  and is indeed quite expensive to precompute (multiple core-days for  $N \approx 80$ , on 2020 hardware). After trying some shortcuts, the current iteration of our code computes these integrals very literally, using the same adaptive Gauss-Kronrod quadrature from the Boost package specified in Chapter 4. A few notes on this precomputation:

1. The integrals  $I_P(\cdot)$  are all analytically integrable and look like (large, complicated) polynomials in  $\sin(\gamma)$  and  $\cos(\gamma)$ . However, already for  $p = q = 20$  the SAGE package seems to give up.
2. There are some more-or-less obvious symmetries which we do not currently exploit.
3. These integrals are somewhat oscillatory, especially for large  $p, q$  and near the boundary of the unit square where Chebyshev functions oscillate the most. A Filon or Levin type quadrature might be much faster. Indeed, we saw some evidence of “thrashing” when running these precomputations.
4. We would ideally want these integrals accurate to machine precision, which is not really something one can guarantee unless the quadrature itself is done in higher precision. Defaulting to 128-bit doubles is probably better, but we have not implemented that. For the lower degree Chebyshev polynomials, Gauss-Kronrod integration should be close to machine accurate anyway.
5. The values of  $I_p(p, q, i, j)$  seem like they might obey a Clenshaw-style recurrence relation for fixed  $i, j$  and versus lower degrees of  $p, q$ . This is motivated by various recurrence formulas for  $T_n$  and its integrals and derivatives, as well as reduction-of-power formulas for integration of powers of trigonometric functions. This would speed up the precomputation (and indeed probably bring it to “real-time”.) However we have not discovered this yet.

### 3.5.2 Chebyshev gyroaveraging: Algorithm

After the above dense matrix is precomputed, the gyroaveraging algorithm is simple:

1. Starting with  $f_{mn}$ , the values of  $f$  sampled at Chebyshev tensor product nodes, perform the below DCT (same as defined above)

$$\hat{f}_{k,\ell} = \sum_{m=0}^{N-1} \sum_{n=0}^{N-1} f_{mn} \cos \frac{m\pi k}{N-1} \cos \frac{n\pi \ell}{N-1}$$

which computes the Chebyshev coefficients (with  $O(N^2 \log(N))$  complexity.)

2. Flatten the above coefficient matrix into a vector with  $N^2$  elements, and apply the precomputed dense  $N^2 \times N^2$  matrix.

The dense multiplication is the bottleneck, and as we see later, can benefit greatly from parallelism (in particular GPU acceleration.) For this algorithm, we expect spectral accuracy for functions which are smooth on the rectangular domain.

# Chapter 4

## Design Considerations

In this chapter we have two main goals: to describe some software engineering objectives and how we achieved them; and to document, in an abbreviated way, the API.

### 4.1 Objectives

From the outset, we intended to build a reusable library that could slip into other numerical solvers easily. To that end, here were some guiding objectives:

1. Performance. The main contribution of this work is dramatically higher performance, without the more drastic step of distributed memory parallelism. To be more precise, we wanted to achieve close to the best performance possible by a non-specialist exercising a “reasonable” amount of effort.
2. Portability and reusability.
3. No “re-inventing the wheel” - in particular, to achieve high-performance, we wanted to use existing highly-tuned libraries that are openly and widely available.
4. Modern idioms for scientific computing - for instance, templates and OOP where they are helpful, and fine-grained control of memory usage only when it is desired.

### 4.2 Design decisions

The space of languages widely used in the scientific community is not so large. For fine-grained memory management and control over performance the most plau-

sible choices are C/C++ and Fortran, and we went with C++. Getting similar performance from Python or Matlab is certainly possible with a great deal of care.

C++ has a mature ecosystem for basic scientific computing, with many libraries available for basic linear algebra. Each of our dependencies is mature and widely installed on scientific computing platforms. With the exception of Boost, they are header-only and can be distributed with our software. Specifically:

1. Boost provides Bessel functions and various Chebyshev-related functionality, and many basic utilities
2. Eigen is a standard library for linear algebra. It is header-only, templated, and handles vectorization, multi-threading, and other performance optimizations for both sparse and dense linear algebra.
3. FFTW is probably the most widely used FFT library, at least in C++.
4. ViennaCL deserves some special mention. ViennaCL is built for sparse linear algebra, specifically on accelerated multi-core platforms (i.e. GPUs and others.) It allows run-time switching between CUDA, OpenCL, and CPU calculation, for both dense and sparse linear algebra, and is competitive with native CUDA in each case. Thus our software has a header-only dependency on ViennaCL, but is fully portable to systems without, e.g., NVIDIA headers or the nvcc compiler.

The other obvious choice for (CPU) linear algebra and FFTs is Intel's MKL. MKL is proprietary, but Eigen has the ability to compile against it, and MKL has an FFTW compatibility layer which one could compile against for moderate performance gains.

Before delving further into implementation decisions, it will be helpful to have a usage example to refer to.



---

```

1  int main(int argc, char* argv[]) {
2      const int N = 64;
3      const int rhocount = 35;
4      const double rhomin = 0.2;
5      const double rhomax = 0.85;
6
7      auto testFunc = [](double rho, double x, double y) -> double {
8          return std::exp(-10 * (x * x + y * y));
9      };
10
11     OOGA::gridDomain g(rhomin, rhomax); //defaults grid to [-1,1]^2
12     OOGA::functionGrid testGrid(g, rhocount, N, false);
13     OOGA::functionGrid exact = testGrid;
14     exact.fillTruncatedAlmostExactGA(testFunc);
15     testGrid.fill(testFunc);
16     auto calctype = OOGA::calculatorType::bicubicDotProductCPU;
17     auto calculator =
18         OOGA::GACalculator<double>::Factory::newCalculator(calctype, g, testGrid);
19     auto result = calculator->calculate(testGrid);
20
21     fftw_cleanup();
22 }

```

---

Listing 1: Minimal usage of gyroaveraging library.

In this listing, we ask for a  $64 \times 64$  grid, using the default domain  $[-1, 1]^2$ . We will do 35 gyroaverages with  $\rho$  varying from 0.2 to 0.85. The function of interest is  $f(\rho, x, y) = e^{-10(x^2+y^2)}$ . Lines 11, 12, and 13 create 2 grids. The function `fillTruncatedAlmostExactGA` performs naive quadrature to evaluate the gyroaverages. Line 15 populates the test grid with sampled function values. Lines 16 and 17 select the calculator type and construct the calculator, and line 19 performs the actual calculation.

The class `functionGrid<class RealT=double>` is not remarkable; it stores vectors for the  $x_i, y_j, \rho_k$  and for the 2d matrix of sampled values. It has methods for printing, norms, finite differencing, and other utilities. It is templated and should support any reasonable floating point type. The underlying data is exposed publicly as a row-major vector and could, for instance, be mapped to an Eigen matrix or other library.

The class `GACalculator<class RealT=double>` is a virtual base class from which each of the actual calculator classes derive. The interface is very simple; construction is restricted to the `Factory::newCalculator` method. There is a

calculate method and a destructor. That’s the whole API in a nutshell.

The constructor for the calculator has the below signature which merits explanation:

```
static std::unique_ptr<GACalculator<RealT>>
newCalculator(calculatorType c, const gridDomain &g, functionGrid<RealT> &f,
fileCache *cache = nullptr, int padcount = 0)
```

The return type is a `std::unique_ptr`. All of the classes in the gyroaveraging package use the RAII (“Resource acquisition is initialization”) idiom for resource management. Specifically, object construction allocates memory, reads pre-computed data from cache, allocates GPU memory, creates GPU handles, etc. All of this is undone by object destruction. The `std::unique_ptr` is a standard C++ way of managing resource intensive objects; it automatically destructs objects when it goes out of scope, and disallows copies. The resources can be manually freed by calling `reset()` on the `std::unique_ptr`. This idiom allows both fine-grained resource management (i.e. user can control exactly when the GPU memory is allocated and freed) as well as code that ignores it altogether (like the example above.)

`calculatorType` is an enum class which chooses the algorithm. Currently exposed are (`linearCPU`, `linearDotProductCPU`, `bicubicCPU`, `bicubicDotProductCPU`, `DCTCPUPaddedCalculator2`, `bicubicDotProductGPU`, `linearDotProductGPU`, `chebCPUDense`, `chebGPUDense`). The next two parameters define the grid. A calculator does all of its precomputation during construction, so a single calculator can only run on a fixed grid size, set of  $\rho_k$ , and domain. Attempting to calculate on a different sized grid will in most cases give a run-time error, but in some cases is undefined behavior. This is not currently checked.

The next parameter is an object which specifies a cache directory for large pre-computed files. All of the classes with significant precomputation allow caching. The default behavior is to try to read a cache file, and if reading fails, to write the cache file. The sizes of the files can be quite large; the testing for this paper generated some 2.5TB of data. The individual sizes are fairly predictable (for instance  $N^4$  doubles for the Chebyshev grids.)

The final parameter is for fine-tuning the padding for the FFT-based algorithm. The default triples the length and width of the grid and this parameter allows for smaller padding if the user is sure it is safe.

Note how the function `testFunc` was defined - while lambdas are certainly expedient, a standard C++ templating trick allows functions to be defined in other ways as well, including the `std::function` wrapper, any object with `operator()` defined, or an old-fashioned function pointer.

Some of the API is hidden behind the scenes, and should be mentioned. The multi-threading is handled by OpenMP, and standard environment variables control how many threads are available to accelerate matrix operations. The potential use of a GPU is enabled by the compile time flag `-DVIENNACL_WITH_OPENCL` and ViennaCL will generally fall back to CPU-based algorithms if it decides it needs to.

At the other end of the API, the dependencies on the FFTW library (and the quadrature and bessel functions of BOOST) are generally contained in an intermediate wrapper function. We were able to swap in various other FFT libraries and quadrature schemes during testing fairly easily due to this extra indirection. Currently we only support floats and doubles for FFT-based algorithms, though larger floating point types are supported on some platforms by FFTW and other FFT libraries.

# Chapter 5

## Numerical Results

### 5.1 Gallery of test functions

In this section we present numerical results, running each gyroaveraging algorithm described above against the below test functions. In each case the domain is the unit square and we tested three values for  $\rho$ :  $\{0.625, 0.46875, 0.875\}$ .

1. The first function is from [6] and has an analytic gyroaverage. The parameter  $A$  is set to 22 so this function has compact support up to machine double precision on the boundary of the unit square.

$$\text{SmoothExp}(x, y) = e^{-A(x^2+y^2)}e^{-B\rho^2}$$

2. The second function is a bivariate version of Runge's function, which is known to cause difficulties for high-degree equispaced polynomial interpolation.

$$\text{SmoothRunge}(x, y) = \frac{(1-x^2)(1-y^2)}{1+25((x-0.2)^2+(y+0.5)^2)}$$

3. Next, we introduce a point singularity. The below horn is continuous but not differentiable at 0.

$$\text{NonsmoothSqrt}(x, y) = \sqrt{(x-0.2)^2+(y+0.5)^2}$$

4. Our next function has 3 non-differentiable kinks, at  $x = y$  and  $|x - y| = 0.75$ .

$$\text{NonsmoothRidge}(x, y) = \max(0, 0.75 - |x - y|)^4(4|x - y| + 1)$$

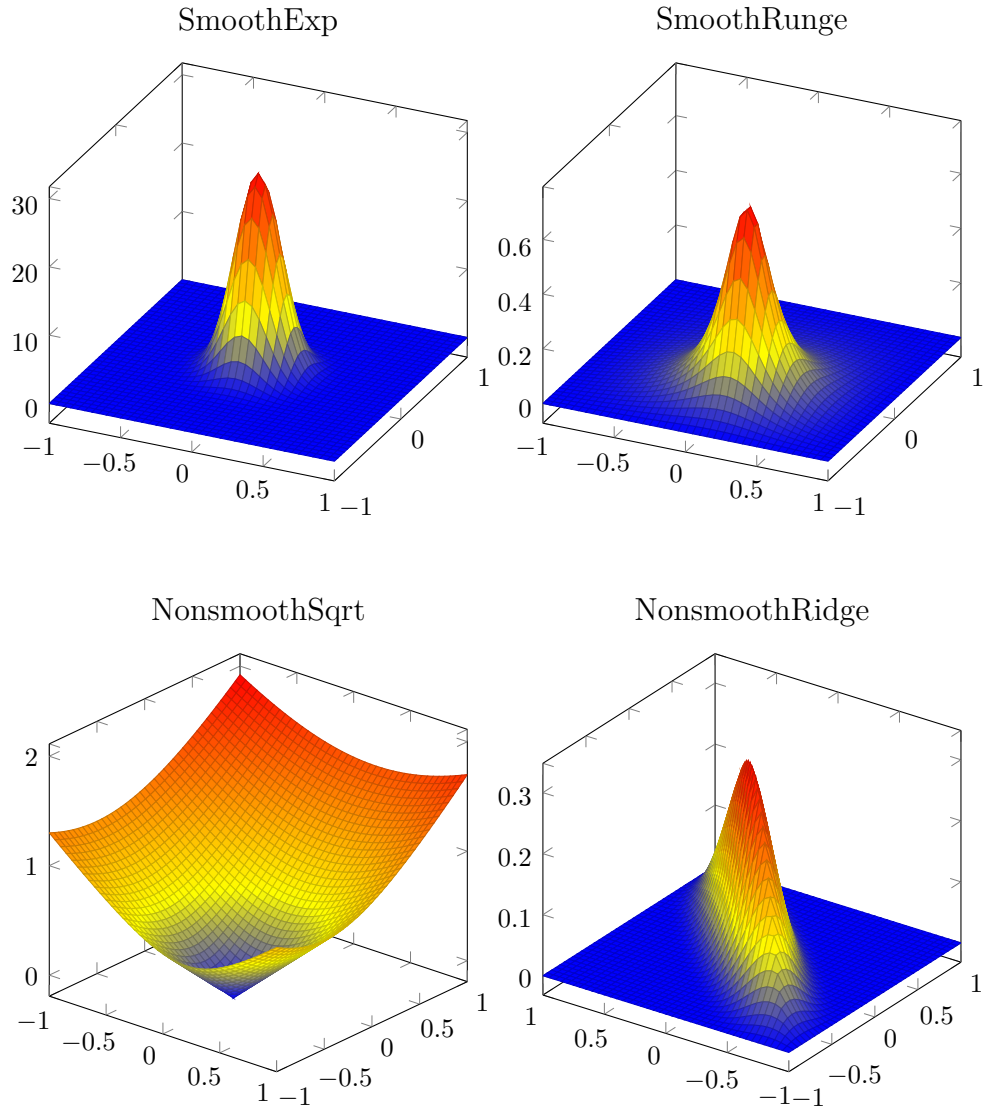


Figure 5.1: Gallery of test functions

## 5.2 Testing environment and setup

The benchmarking process is outlined below:

1. First, each algorithm is run on each function to completion for increasing  $N$  until a memory exception is triggered. This has two effects
  - (a) Precomputed matrices for the sparse and dense matrix-vector product algorithms are generated and cached

- (b) Precomputed benchmark gyroaverage for each function and  $N$  is generated and cached. This is calculated straight from the definition using black-box Gauss-Kronrod quadrature from the Boost C++ library. For the smooth functions this was verified to be correct within one digit of machine precision vs a double-precision analytic calculation.
2. After a complete precomputation step, for each triple of (algorithm, function,  $N$ ),
- (a) Run a single gyroaverage calculation, to warm up cache, and force initialization of GPUs and compilation of GPU machine code
  - (b) Rerun the gyroaverage calculation, benchmarking the wall-clock time
  - (c) storing the a vector of errors for each value of  $\rho$ . The error is defined, given matrices  $f'_{ij}$  the approximation and  $\hat{f}_{ij}$  representing the benchmark, as

$$\frac{\max_{i,j} |\hat{f}_{ij} - f'_{ij}|}{\max_{i,j} |\hat{f}_{ij}|}$$

The benchmarks were run on the NYU Greene supercomputing cluster around December 2020, using two different classes of nodes. The CPU nodes are 48 cores (2 2.9Ghz Intel Xeon 24C CPUs) with 192Gb of memory. The GPU nodes are additionally equipped with 4 RTX8000 GPUs. We used, for our testing, a single GPU at a time and a maximum of 20 cores. In all cases the input data and output data are held in CPU memory and the full penalty of GPU memory transfer is included in the benchmarks.

## 5.3 Performance and Convergence Plots

See below for numerical results; the plots are intended to speak for themselves. Figure 5.2 presents the performance scaling properties of each algorithm. Figure 5.3 present convergence scaling properties, which depend strongly on the smoothness of the initial data. Figure 5.4 attempts to show an “efficient frontier” for the trade-off between accuracy and speed.

## 5.4 Discussion of numerical results

First, as a reference point, it will be useful to refer to [6, P. 16]. The author describes a single gyroaverage calculation (for 35 values of  $\rho$ ) of the same “Smooth Exponential” function we have used, to accuracy  $10^{-13}$ , taking approximately 13

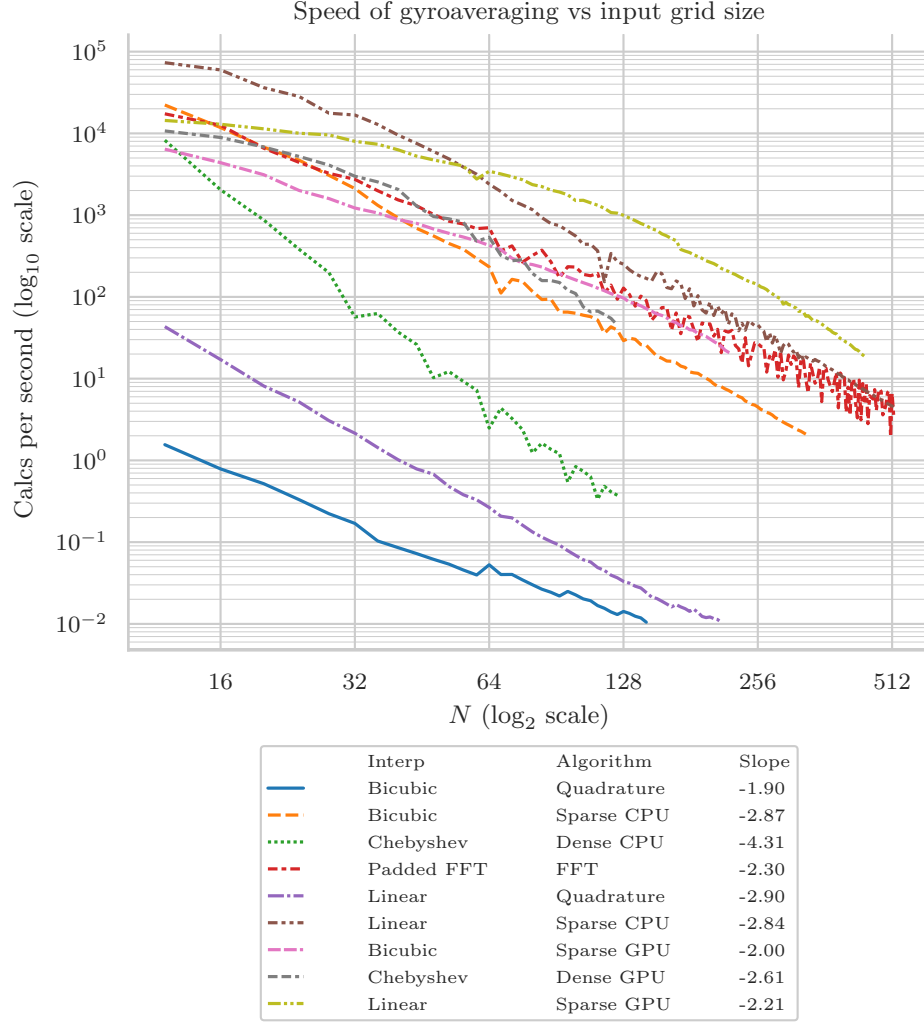


Figure 5.2: Calculation speed as grid size grows. The slope is a linear regression coefficient for the displayed log-log plot. Note that while the CPU-bound Chebyshev algorithm exhibits worse than quartic scaling, the GPU version scales with lower exponent (-2.61); this reflects the significance of the cost of CPU-GPU memory transfer which scales like  $N^2$ .

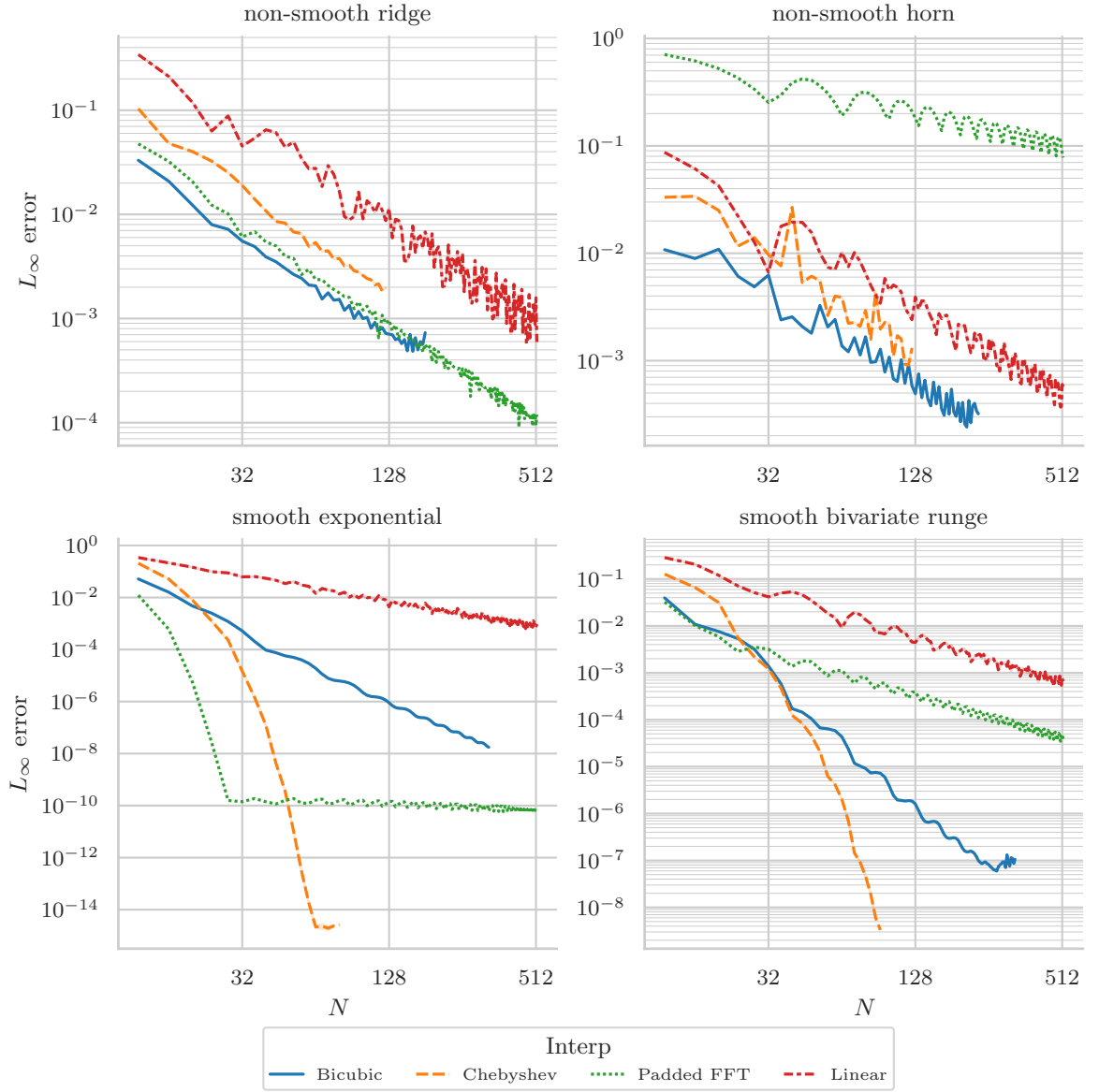


Figure 5.3: Error vs grid size. By construction, no one algorithm is a clear winner. For smooth functions, we get spectral accuracy from the Chebyshev interpolation, and the Fourier method as well in the numerically periodic case.



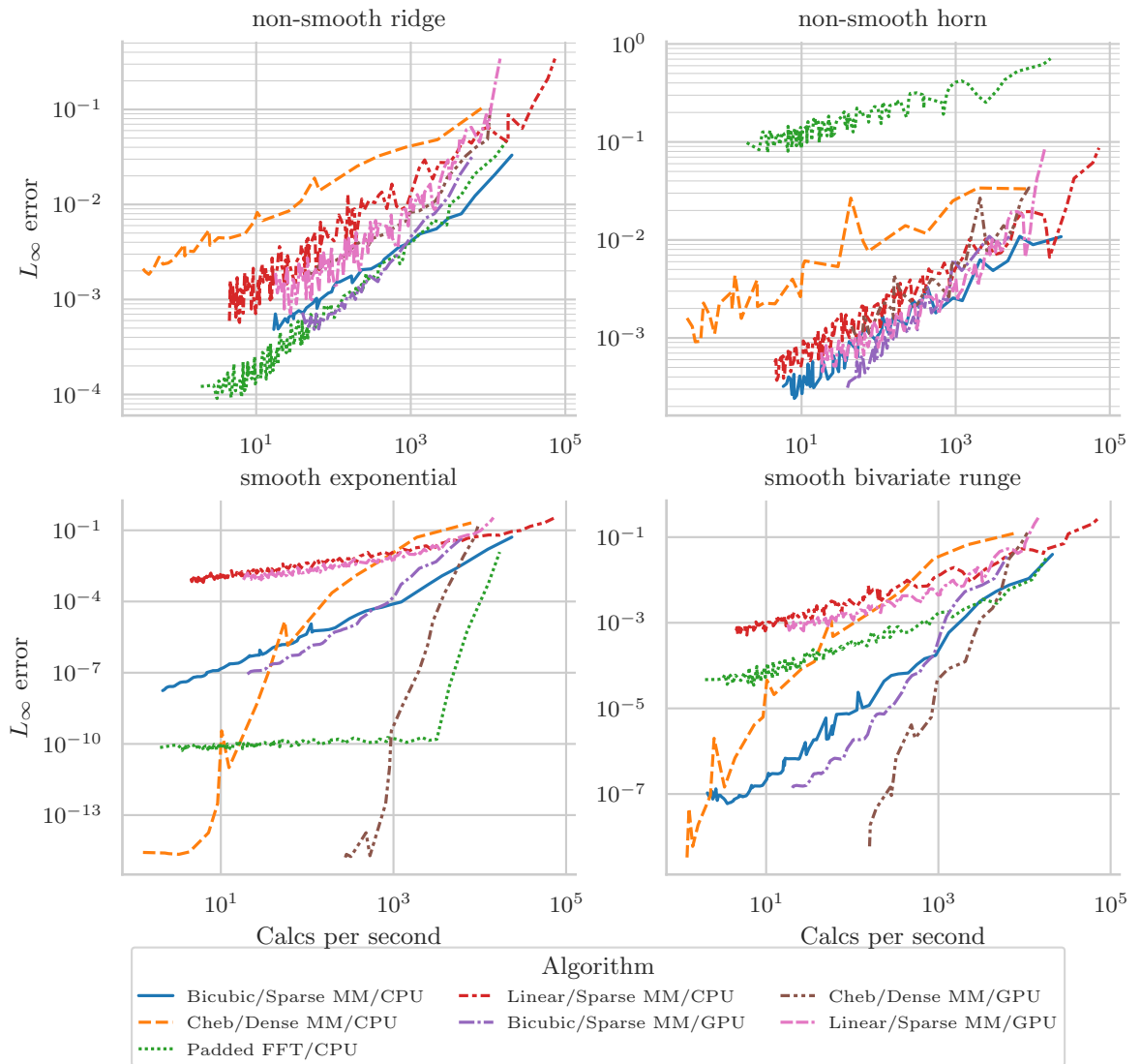


Figure 5.4: The trade-off between accuracy and execution speed.

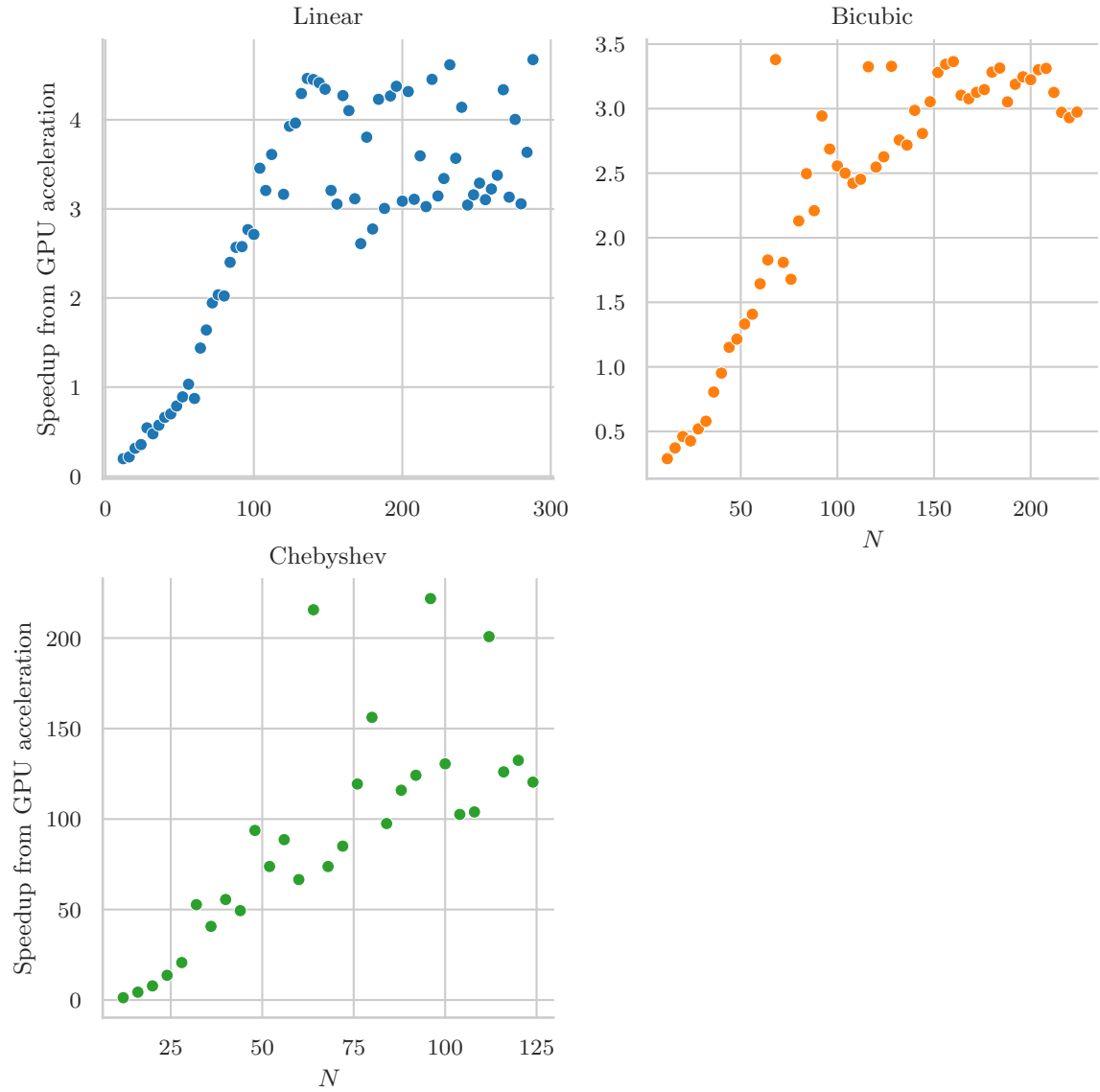


Figure 5.5: The speed benefit of GPU parallelism. These acceleration ratios are typical for sparse vs. dense linear algebra. This includes the full penalty of CPU-GPU memory transfer in both directions.

seconds. To be clear, [6] was not focused on performance, and notes various potential improvements including parallelization.

This work has gained 3-4 orders of magnitude performance increase for similar accuracy on this smooth function. We can trace this to a few different sources, including: 1) Matlab vs C++, 2) multi-core CPU parallelism, 3) GPU acceleration in some cases.

However, both [5] and [6] present FFT-based methods, which are not expected to converge well for non-smooth functions, nor for functions which are not numerically of compact support. Except for the “smooth exponential” function, the bicubic interpolation and Chebyshev based algorithms are competitive with respect to both accuracy and speed with the padded FFT algorithm. Indeed, as expected, the bicubic interpolation is most robust to the “horn” singularity. On the other hand, the Chebyshev interpolation alone is able to demonstrate spectral accuracy for the non-compactly supported “Runge” function.

# Chapter 6

## Conclusion

### 6.1 Proof of concept

We can conclude from the previous chapter three main points:

1. As a proof of concept, the bicubic and bilinear interpolation schemes for gyroaveraging were successfully translated into sparse linear algebra operations, and parallelized/accelerated using existing state-of-the-art linear algebra libraries.
2. These schemes were shown to be competitive with spectral methods when, for instance, singularities make the advantages of spectral methods moot.
3. All methods were implemented efficiently so that  $10^3$  gyroaverage calculations could be achieved per second on a single machine (with, admittedly, expensive hardware.) This required in some cases reframing the discretization so that GPU acceleration could be brought to bear on the problem.

### 6.2 Further development

There are many avenues for further testing and development, including:

1. Distributed memory parallelism: Both dense and sparse linear algebra are easily distributed on an HPC grid. Since the main operation of our algorithms is a single large fixed matrix applied to a relatively small vector, the communication bottleneck should not be severe and all algorithms might scale quite well.
2. Faster and more accurate precomputation of the dense Chebyshev matrix, as described in 3.5.1.

3. “Low rank” Chebyshev representations of functions: The Chebfun2 package, as described in [9] documents an efficient way to calculate low-rank representations of bivariate functions with the same Chebyshev basis functions we use. Such low-rank approximations would require only a small portion of the  $N^4$  matrix we use, though we would still have to precompute the whole thing. Easier would be filtering the results of the DCT (i.e. very small Chebyshev coefficients) or, perhaps, throwing out the bottom right half of the Chebyshev coefficients (i.e. high frequency mixed modes.)
4. Adaptivity. By using adaptive refinement but on fixed precomputed grids, one could choose the  $N$  to approximate the input to some tolerance, and insure a similar tolerance for the gyroaverages. This is already non-trivial for the equispaced grids and may not work for Chebyshev.
5. Integration into a fully GPU workflow: FFTs, finite differencing, and even Poisson solving are all available for GPUs. For each of the gyroaveraging applications mentioned in the introduction, it is possible that one could avoid GPU-host memory transfer by doing all of the work (including time-stepping or other iteration) on the GPU device. This is of course very application dependent.

# Bibliography

- [1] *Bessel Function*. In: *Wikipedia*. Feb. 8, 2021. URL: [https://en.wikipedia.org/w/index.php?title=Bessel\\_function&oldid=1005618018](https://en.wikipedia.org/w/index.php?title=Bessel_function&oldid=1005618018) (visited on 02/15/2021).
- [2] “NIST Digital Library of Mathematical Functions”. In: (). URL: <http://dlmf.nist.gov/,%20Release%201.1.0%20of%202020-12-15>.
- [3] Yiqiu Dong, Torsten Görner, and Stefan Kunis. “An Algorithm for Total Variation Regularized Photoacoustic Imaging”. In: *Advances in Computational Mathematics* 41.2 (Apr. 2015), pp. 423–438. ISSN: 1019-7168, 1572-9044. DOI: 10.1007/s10444-014-9364-1. URL: <http://link.springer.com/10.1007/s10444-014-9364-1> (visited on 02/11/2021).
- [4] Lawrence C. Evan. *Partial Differential Equations by Lawrence C. Evans*. AMS, 2010., Jan. 1, 2010.
- [5] Torsten Görner, Ralf Hielscher, and Stefan Kunis. “Efficient and Accurate Computation of Spherical Mean Values at Scattered Center Points”. In: *Inverse Problems & Imaging* 6.4 (2012), p. 645. DOI: 10.3934/ipi.2012.6.645. URL: <https://www.aims sciences.org/article/doi/10.3934/ipi.2012.6.645> (visited on 02/11/2021).
- [6] Joseph Guadagni and Antoine J. Cerfon. *Fast and Spectrally Accurate Evaluation of Gyroaverages in Non-Periodic Gyrokinetic-Poisson Simulations*. July 5, 2017. arXiv: 1707.01260 [physics]. URL: <http://arxiv.org/abs/1707.01260> (visited on 02/11/2021).
- [7] J. C. Mason and David C. Handscomb. *Chebyshev Polynomials*. 1st edition. Boca Raton, Fla: Chapman and Hall/CRC, Sept. 17, 2002. ISBN: 978-0-8493-0355-5.
- [8] Theodore J. Rivlin. *Chebyshev Polynomials: From Approximation Theory to Algebra and Number Theory*. 2nd edition. New York: Wiley-Interscience, June 1, 1990. 249 pp. ISBN: 978-0-471-62896-5.

- [9] Alex Townsend and Lloyd N. Trefethen. “An Extension of Chebfun to Two Dimensions”. In: *SIAM Journal on Scientific Computing* 35.6 (Jan. 1, 2013), pp. C495–C518. ISSN: 1064-8275. DOI: 10.1137/130908002. URL: <https://epubs.siam.org/doi/10.1137/130908002> (visited on 02/17/2021).
- [10] Lloyd N. Trefethen. *Approximation Theory and Approximation Practice, Extended Edition*. Other Titles in Applied Mathematics. Society for Industrial and Applied Mathematics, Jan. 1, 2019. 364 pp. ISBN: 978-1-61197-593-2. DOI: 10.1137/1.9781611975949. URL: <https://epubs.siam.org/doi/book/10.1137/1.9781611975949> (visited on 02/11/2021).
- [11] Felipe Vico, Leslie Greengard, and Miguel Ferrando. “Fast Convolution with Free-Space Green’s Functions”. In: *Journal of Computational Physics* 323 (Oct. 15, 2016), pp. 191–203. ISSN: 0021-9991. DOI: 10.1016/j.jcp.2016.07.028. URL: <https://www.sciencedirect.com/science/article/pii/S0021999116303230> (visited on 02/17/2021).